

Received February 28, 2018; reviewed; accepted March 21, 2018

## Contribution on fluid inclusion abundance to activation of quartz flotation

Yunru Yuan <sup>1</sup>, Lingyan Zhang <sup>1,2</sup>, Junfang Guan <sup>1,2</sup>, Chong Zhang <sup>3</sup>, Jianxin Wu <sup>3</sup>, Zhiqiang Chen <sup>3</sup>

<sup>1</sup> School of Resources and Environmental Engineering, Wuhan University of Technology, Wuhan 430070, China

<sup>2</sup> Hubei Key Laboratory of Mineral Resources Processing & Environment, Wuhan 430070, China

<sup>3</sup> Bengbu Design & Research Institute for Glass Industry, Bengbu 233018, Anhui, China

Corresponding author: zhly@whut.edu.cn (Lingyan Zhang)

**Abstract:** In this study, comparative experiments were conducted on the recovery of quartz using flotation with different fluid inclusion abundances. A large number of fluid inclusions with various sizes have been found in natural quartz. Micrographs, inductively coupled plasma, electron probe microanalysis, homogenization temperature, Raman spectra, zeta potentials, X-ray photoelectron spectroscopy, scanning electron microscope, and energy dispersive spectrometer were used to characterize the fluid inclusions and quartz, as well as the adsorption tests and single mineral flotation experiments to investigate its floatability. The results demonstrated that it was more likely for quartz with higher fluid inclusion abundance to connect with Fe<sup>3+</sup> sufficiently to achieve a high level of flotation recovery, due to the powerful collecting ability by sodium dodecyl sulphonate to Fe<sup>3+</sup>. Furthermore, the mechanism indicated that the adsorption between quartz and Fe<sup>3+</sup> was a process of chemisorption.

**Keywords:** Fly ash, rotary triboelectrostatic separator, plate voltage, numerical simulation

### 1. Introduction

Quartz whose crystal formula is SiO<sub>2</sub> belongs to hexagonal crystal system and it is abundant in the Earth's crust in igneous, metamorphic, and sedimentary rocks. Quartz is a kind of silicate mineral resources with very stable physical and chemical properties. High purity quartz is widely used as an irreplaceable raw material in the high-tech industry (Vatalis et al., 2015; Platias et al., 2013) including the semi-conductor technologies, high temperature lamp tubing, telecommunication, optics (Santos et al., 2015). With the rapid development of the technique of electronic information, quartz becomes more and more important nowadays. However, the highly pure quartz found in the world becomes less and poorer in the future.

There are several processing methods to reduce the impurities in quartz, including physical and chemical treatments (Veglio et al., 1999; Tuncuk et al., 2016; Li et al., 2010). In conventional methods, magnetic separation (Nie et al., 2013), flotation (Sahoo et al., 2013) and acid leaching (Zhang et al., 2012; Du et al., 2011) are used to remove impurities from silica sand ore. Flotation is an important and vital method to separate valuable minerals from gangue effectively (Chandra et al., 2009). Many researchers have proved that flotation is an efficient technique to concentrate quartz (Wang et al., 2005; Mowla et al., 2008). It was studied by Larsen et al. (2015) that quartz could be floated in diluted solutions of hydrofluoric acid (HF) simply by the aid of frothers alone. However, flotation is affected by many factors, such as pH of the pulp, types of collectors and activators, dosage of collector and activator, time and temperature (Xia, 2017). Moreover, one of the most important factors affecting the flotation performance of minerals is the surface morphology, including roughness, roundness, contact angle, and shape etc (Koh et al., 2009). Vaziri Hassas et al. (2016) suggested that increasing the surface roughness

of glass beads could improve the flotation recovery, contact angle, and bubble attachment. Krasowska et al. (2007) studied that roughness itself could reduce the induction time, as well as the bubble bounce on the surface prior to attachment. In addition, one of the factors affecting the surface characteristics of quartz is the content of fluid inclusions.

Inclusions come into being because of the defects in crystal during the complete crystallization of mineral crystals (Lu et al., 2004). The first-hand information on fluids in the Earth's interior can be obtained by studying fluid inclusions (Luce et al., 2012). Fluid inclusions can be classified into primary inclusions, pseudo secondary inclusions and secondary inclusions according to their forming causes (Van Den Kerkhof et al., 2001). Fluid inclusions are generally small closed volumes, and their components can be characterized by Raman spectroscopy (Burke, 2001). Also, the morphology of the fluid inclusions can be researched by microscope observation of a thin section of the target mineral (Xu J.G., 1991).

As previously reported in the literature (Goldstein, 2001), fluid inclusions prevalently exist in natural minerals. Moreover, there are large numbers of fluid inclusions with various sizes in quartz. The effect of the components released from the fluid inclusions on their flotation performance was investigated in reported papers recently, as well as other research progress on fluid inclusions (Hou et al., 2012; Liu et al., 2013). However, limited studies have focused on the effect of inclusion abundance on the surface characteristics of quartz, which directly affects the flotation results.

In this study, a comparison of the recovery of quartz via flotation with different fluid inclusion abundance was investigated, revealing the influence of fluid inclusions on the flotation behavior of quartz.

## 2. Experimental

### 2.1 Materials and chemicals

Hand-picked natural pure specimens of two types of  $\alpha$ -quartz with different fluid inclusions, labeled as 1# and 2#, were obtained from Anhui province in China. The samples were ground via a pottery ball mill and the 38-75  $\mu\text{m}$  fractions were used in flotation tests. The silicon dioxide content of 1# and 2# is above 99.6%. The chemical composition of samples used for the study was shown in Table 1. Iron (III) chloride hexahydrate, sodium dodecyl sulphonate (SDS), rhodamine B (RhB), potassium periodate, and sodium hydroxide, all of analytical purity, along with sulfuric acid (98%) and hydrochloric acid (36%) were all purchased from Sinopharm Chemical Reagent Co., Ltd, China. The deionized water used in this work was produced by a Milli-Q Direct 16 with a resistivity of 18.25  $\text{M}\Omega\text{ cm}$ .

Table 1. Chemical composition of minerals (wt.%)

Samples	$\text{Al}_2\text{O}_3$	$\text{CaO}$	$\text{Fe}_2\text{O}_3$	$\text{K}_2\text{O}$	$\text{Na}_2\text{O}$	$\text{SO}_3$	$\text{SiO}_2$
1#	0.0929	0.0744	0.0580	0.0405	0.0212	0.0016	99.6075
2#	0.0625	0.0676	0.0561	0.0656	0.0098	0.0269	99.6272

### 2.2 Flotation tests

Flotation tests of each quartz (7 g) were conducted using a RK/FGC5-35 flotation machine with a spindle speed of 2060 r/min. The reagents were added in the following order: (a)  $\text{Fe}^{3+}$  ( $7 \times 10^{-4}$  mol/l) conditioning for 3 min; (b) HCl or NaOH conditioning for 3 min; (c) SDS ( $9 \times 10^{-4}$  mol/l) conditioning for 3 min, followed by flotation collection period for 4 min. No frother was used in the flotation tests due to the frothing action of SDS. The products were weighed and tested after filtration and drying, and used to calculate the recovery. The equation was expressed as following:

$$R(\%) = \frac{m_1}{m_1 + m_2} \times \frac{\beta}{a} \times 100 \quad (1)$$

where  $R$  (%) is the flotation recovery,  $m_1$  (g) is the mass of flotation froth products,  $m_2$  (g) is the mass of the remaining products in the flotation cell,  $\beta$  (%) is the concentrate grade, and  $a$  (%) is the grade of samples.

## 2.3 Measurements

Inductively Coupled Plasma Atomic Emissions Spectrometry (ICP-AES, Optima4300DV, Perkin Elmer Ltd., America) was used to determine the chemical compositions of samples and flotation concentrate. Micrographs of the ore were obtained using a Leica microscope (DMLP S8APO, Germany) coupled with a digital camera. Components of samples were observed by electron probe microanalysis (EPMA, JXA-8230, JEOL Ltd., Tokyo, Japan). The homogenization temperature of the fluid inclusions in samples was measured by heating-freezing stage (Linkan THMS-600, England). Measurement has precision better than  $\pm 1$  °C and  $\pm 0.1$  °C in the temperature ranges of -200 to 400 °C and -30 to 50 °C, respectively. A Renishaw INVIA Raman microscope (Renishaw Corporation, Gloucestershire, England) was used to obtain the Raman spectra of the fluid inclusions in quartz ore within the Raman shift range of 500–3000  $\text{cm}^{-1}$ , using an Ar laser probe at the 514.5 nm mode. The zeta potentials of minerals were measured by a JS94H micro electrophoresis instrument (Shanghai Zhongchen Digital Technic Apparatus Co., China). X-ray photoelectron spectroscopy (XPS) of the samples was performed using a VG Multilab 2000 (Thermo Electron Corporation, Waltham, MA, USA) with a monochromatic Al X-ray source operating at 300W. Scanning electron microscope (SEM, JSM-5610LV, JEOL Ltd., Japan) and energy dispersive spectrometer (EDS, Phoenix, EDAX, USA) were used to find the broken areas of fluid inclusions and study the composition of the regions. The SDS in the flotation filtrate was mixed with RhB, potassium periodate, and sulfuric acid to be examined by a UV spectrophotometer (A360, Shanghai AOE Instruments Co., Ltd, Shanghai, China) at a wavelength of 552 nm (Zhai, 2010).

## 3. Results and discussion

### 3.1. Mineralogy of quartz

#### 3.1.1 Optical microscope analysis of quartz

Micrographs of the quartz samples were shown in Fig. 1. As shown in Fig. 1(b, d), there were no obvious gangue minerals except a little mineral assemblage of muscovite in quartz particles. As shown in Fig. 1(a, c), clay minerals and fluid inclusions were distributed along the quartz grain boundaries. Moreover, the surface of 2# was cleaner than that of 1#.

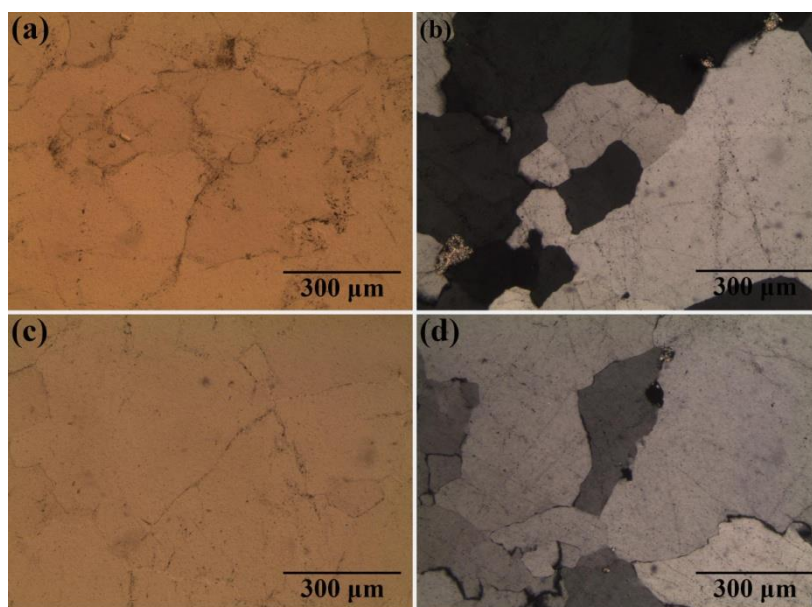


Fig. 1. Micrographs of quartz samples: (a) micrograph of 1# with single polarization; (b) micrograph of 1# with crossed polars; (c) micrograph of 2# with single polarization; (d) micrograph of 2# with crossed polars

#### 3.1.2 Electron probe microanalysis

Microprobe slices of the two samples were analyzed and 70 spots of samples were detected in total. There were no impurity elements detected in the microprobe slices, and the content of  $\text{SiO}_2$  on these

points was all 100%. The results showed that the compositions of the two quartz samples were single, and the impurity elements were mainly hosted in gangue minerals.

### 3.2 Fluid inclusions

#### 3.2.1 Morphology of fluid inclusions in quartz

The morphology of fluid inclusions in 1# and 2# obtained by microscopy is shown in Fig. 2, respectively. As shown in Fig. 2(a-d), large numbers of fluid inclusions with various sizes were observed in the thin section of 1#. Most of the large inclusions were in irregular shape, while the small inclusions were usually elliptical. The sizes of fluid inclusions ranged from several microns to several dozens of microns, among which the largest size and smallest size were 25.988  $\mu\text{m}$  and 1.941  $\mu\text{m}$ , respectively. As shown in Fig. 2(e-h), few fluid inclusions can be observed in the thin section of 2#. Most fluid inclusions were two-phase isolated primary inclusions and chained secondary inclusions along fractures in quartz particles. The sizes of fluid inclusions varied slightly, among which the sizes ranged from 5.349  $\mu\text{m}$  to 12.380  $\mu\text{m}$  in general.

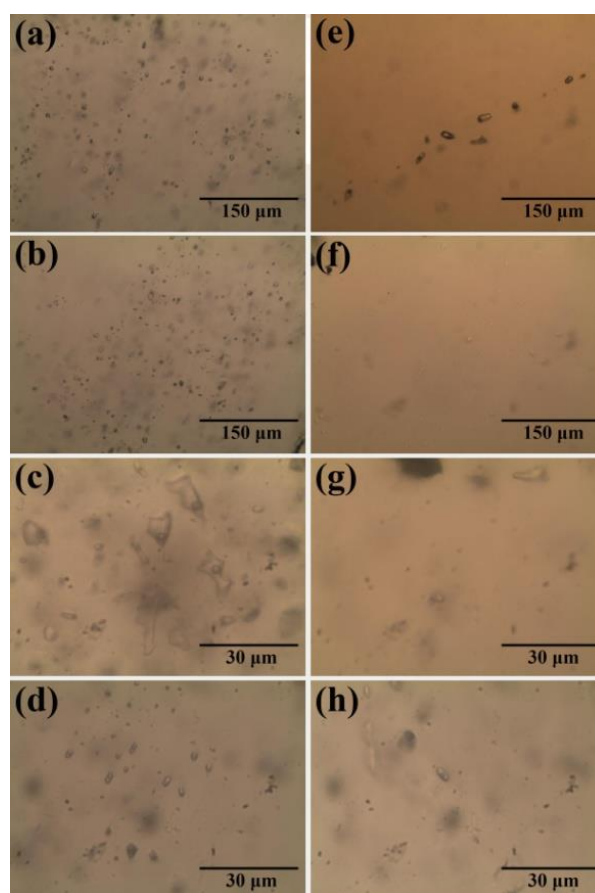


Fig. 2. Micrograph of fluid inclusions in quartz: (a-d) inclusions in 1#; (e-f) inclusions in 2#

On the basis of the previous study, the fluid inclusion abundance can be calculated according to the following equation (Lu et al., 2004):

$$A(\%) = \frac{nV_1}{V_0} \times 100 \quad (2)$$

where  $A(\%)$  is the fluid inclusion abundance,  $V_0$  is the volume of the measured quartz particle,  $V_1$  is the average volume of the fluid inclusions in the measured quartz particle, and  $n$  is the number of fluid inclusions in the measured quartz particle.

According to the sizes and numbers of fluid inclusions measured by the microscope, the fluid inclusion abundances were 0.42% for 1# and 0.11% for 2#, indicating that there was a difference in

characteristic properties on the surface of the samples attributed to the various fluid inclusion abundances.

### 3.2.2 Fluid inclusion microthermometry

The temperature measurement results of two samples are illustrated in Fig. 3. Histogram was drawn using the homogenization temperatures of two quartz samples. The fluid inclusions in 1<sup>#</sup> were mainly the gas-liquid aqueous inclusions. The ice melting temperature of the gas-liquid aqueous inclusions was from -7.2 to -0.2 °C. The homogenization temperature is in the range of 80–210 °C, and concentrated in the range of 120–160 °C. The temperature was homogenized to liquid phase. Using the reference data of Bodnar for the NaCl-H<sub>2</sub>O system (Bodnar, 1993), the calculated salinity was in the ranges of 0.35%–10.73% (mass fraction, NaCl<sub>eq</sub>). According to the morphology of fluid inclusions in 2<sup>#</sup>, the fluid inclusions in 2<sup>#</sup> were also the gas-liquid aqueous inclusions in general. The ice melting temperature of the gas-liquid aqueous inclusions was from -9.5 to -1.7 °C. The homogenization temperature is in the range of 80–290 °C, and concentrated in the range of 160–200 °C. The calculated salinity was in the ranges of 2.90%–13.40% (mass fraction, NaCl<sub>eq</sub>). 1<sup>#</sup> and 2<sup>#</sup> inclusions had similar homogenization temperatures concentrated in the range of 120–200 °C and salinities, indicating that the ore-forming conditions of the two quartz samples were similar.

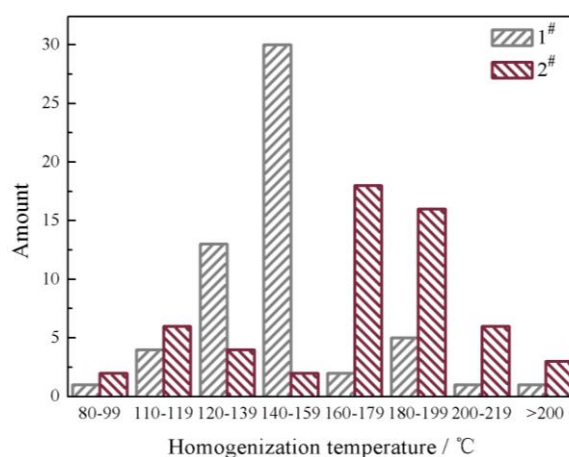


Fig. 3. Homogenization temperature of fluid inclusions

### 3.2.3 Raman analysis

At room temperature, the inclusions in quartz were mainly in the gas-liquid phase, and the components of inclusions were characterized by Raman spectra. It can be seen from Fig. 4, the liquid phase of inclusions was generally H<sub>2</sub>O, whose peak located at approximately 3409 cm<sup>-1</sup> (Dubessy et al., 1992). The peaks of CO<sub>2</sub> were at around 1284 cm<sup>-1</sup> and 1388 cm<sup>-1</sup>, indicating the gas phase of inclusions was CO<sub>2</sub> in general (Paris-nord et al., 1989). As seen in Fig. 4, the two types of quartz have similar fluid inclusions in composition. In addition, due to the simple composition of inclusions, few ions released to the flotation pulp when the inclusions were broken open during the grinding process, which could hardly affect flotation results.

### 3.3 Zeta potential

As shown in Fig. 5, the surface of quartz possessed negative charges over the pH range of 2 to 10, indicating that they were attractive to cations. The PZC of 1<sup>#</sup> and 2<sup>#</sup> were found to be pH 2.0 and 2.2, respectively, which were consistent with reported studies (Huang et al., 2001; Wang et al., 2005). The greatest negative charges of 1<sup>#</sup> and 2<sup>#</sup> appeared at pH 9.0, which were -60.24mV and -57.63mV respectively. During the grinding process of quartz, a certain amount of Si-O bonds are broken, and -Si-O- and -Si<sup>+</sup> sites generated (Luo et al., 2015). Due to the larger fluid inclusion abundance for 1<sup>#</sup>, more Si-O bonds were broken and more OH<sup>-</sup> ions adsorbed onto the quartz's surface that resulted in the lower zeta potential than that of 2<sup>#</sup>.

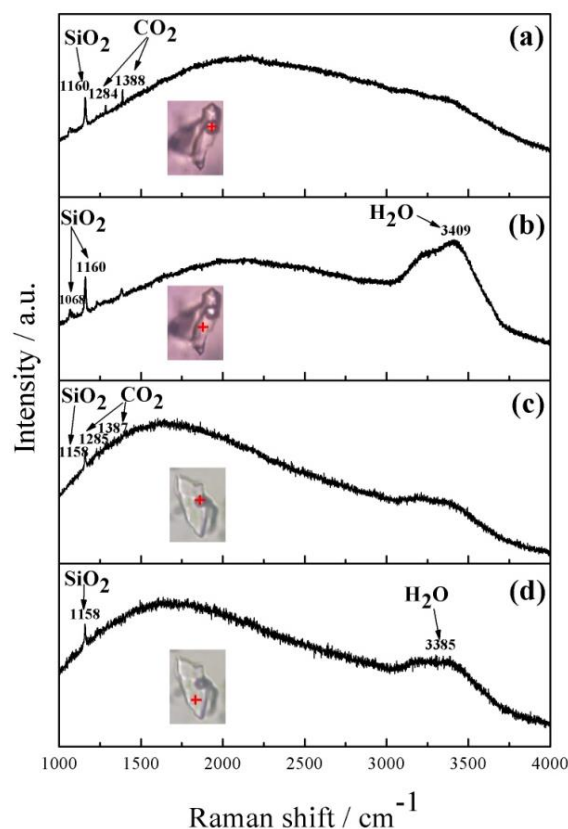


Fig. 4. Raman patterns of fluid inclusions in quartz: (a-b) inclusion in 1<sup>#</sup>; (c-d) inclusion in 2<sup>#</sup>

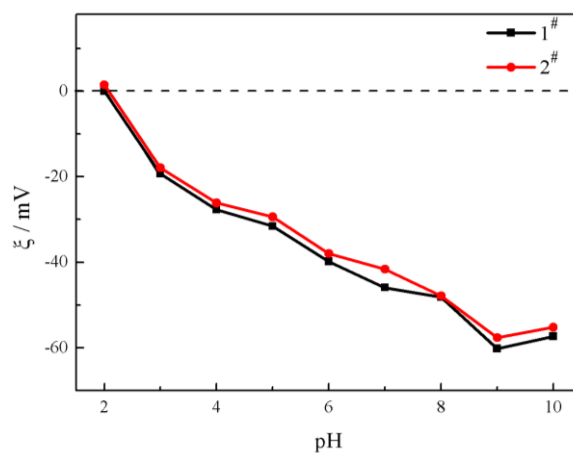


Fig. 5. Zeta-potentials of 1<sup>#</sup> and 2<sup>#</sup> as a function of pH

### 3.4 XPS results

The results of XPS survey spectra of the samples treated and untreated by Fe<sup>3+</sup> were shown in Fig. 6. Due to the high purity of 1<sup>#</sup> and 2<sup>#</sup>, two peaks centered at 110.65 eV and 545.65 eV were observed, corresponding to the Si 2p and O 1s, respectively. In addition, the presence of Fe 2p peaks was confirmed from the spectra after treated by Fe<sup>3+</sup>, verifying the effectiveness of the adsorption reaction. On the whole, in addition to the slight increase on the peak intensity of Fe 2p after reaction, XPS spectra of quartz showed hardly obvious change before and after the treatment of Fe<sup>3+</sup>.

To further investigation of the adsorption of Fe<sup>3+</sup> on quartz surface, the XPS Fe (2p) spectra of samples and surfaces treated with FeCl<sub>3</sub> solution were recorded and the results were summarized in Fig. 7 and Table 2. The element of Fe on 1<sup>#</sup> surface varied from 0.29% to 1.67%, while that of 2<sup>#</sup> varying from 0.26% to 1.53% after treated by Fe<sup>3+</sup>. The difference on Fe atomic concentration with treatment or not were 1.38% and 1.27% for sample 1<sup>#</sup> and 2<sup>#</sup>, respectively, indicating that the surface of sample 1<sup>#</sup>

adsorbed more Fe element effectively. With regard to sample 1#, the binding energy of Fe 2p displayed a shift from 713.36 eV to 711.52 eV after the adsorption of Fe(III) on quartz, implying that a coordination reaction of Fe(III) could take place on the surface of quartz (Fan et al., 2012). In addition, the binding energy of O 1s was observed at 532.63 eV, which was 0.12 eV lower than that before reaction. The decrease on the binding energy of O 1s occurred attributed to the covalent combination between Fe(III) and O in the Si-O-Si (Allen, 2004), similar to the results of sample 2#.

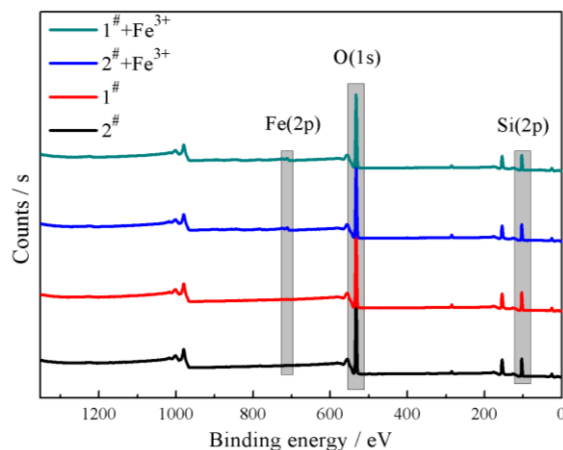


Fig. 6. XPS survey spectra of the samples treated and untreated by Fe<sup>3+</sup>

Fe<sup>3+</sup> can be adsorbed on the mineral surface with the form of hydroxide or hydroxyl complex by chemical bonding force and electrostatic force. Therefore, the adsorption ability of Fe<sup>3+</sup> on mineral surface is closely related to the content of surface anionic O<sup>2-</sup>. The higher the content of O<sup>2-</sup> on the mineral surface is, the stronger negative potential of the surface can possess. Moreover, surface with negative potential could increase the adsorption ability of Fe<sup>3+</sup>, beneficial to intensify the activation of Fe<sup>3+</sup> to quartz. And the presence of larger fluid inclusion abundance and negative potential of sample 1# resulted in more Fe element appeared on the surface.

Table 2. XPS characterization of reference compounds

Samples	Elements	Untreated		Treated by Fe <sup>3+</sup>	
		Binding energy (eV)	Percentage (%)	Binding energy (eV)	Percentage (%)
1#	Fe	713.36	0.29	711.52	1.67
	O	532.75	62.95	532.76	62.5
2#	Fe	713.29	0.26	711.49	1.53
	O	532.63	61.56	532.71	61.23

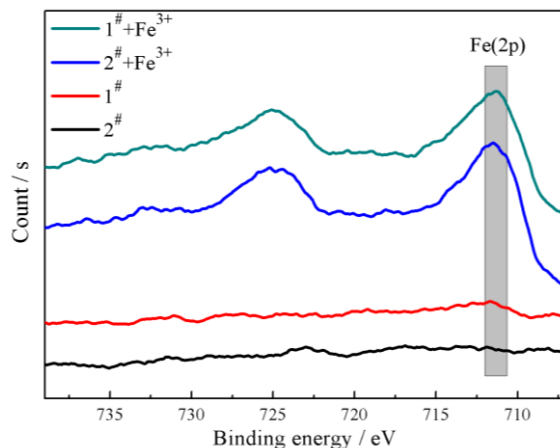


Fig. 7. XPS Fe (2p) spectra of samples treated and untreated by Fe<sup>3+</sup>

### 3.5 SEM/EDS results

Fig. 8 showed the SEM and EDS results of the surface of the samples after being treated by  $\text{Fe}^{3+}$ . For comparison, the positions chosen for EDS analysis were shown by the crosses in Fig. 8(a, d): the broken regions (b, e) and the flat areas (c, f). Due to broken fluid inclusions or the scratches caused during sample preparation, some broken regions with various shapes existed on the quartz surface. As shown in Fig. 8, the concentrations of Fe at position b and c were 0.09 and 0.03 wt%, which indicated that more  $\text{Fe}^{3+}$  was adsorbed on broken areas of fluid inclusions rather than on flat areas. What's more, the EDS results of 2# also showed the same rule. Thus, the content of fluid inclusions in quartz had an effect on the adsorption ability of  $\text{Fe}^{3+}$ , in good agreement with the XPS results.

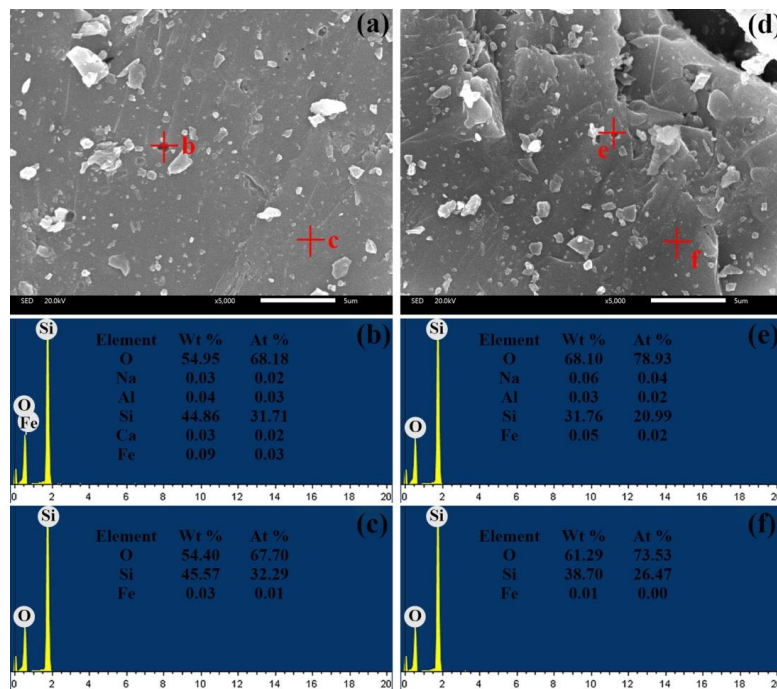


Fig. 8. SED and EDS results of samples treated by  $\text{Fe}^{3+}$ : (a) surface morphology of 1#; (d) surface morphology of 2#; (b, c, e, f) correspond to positions

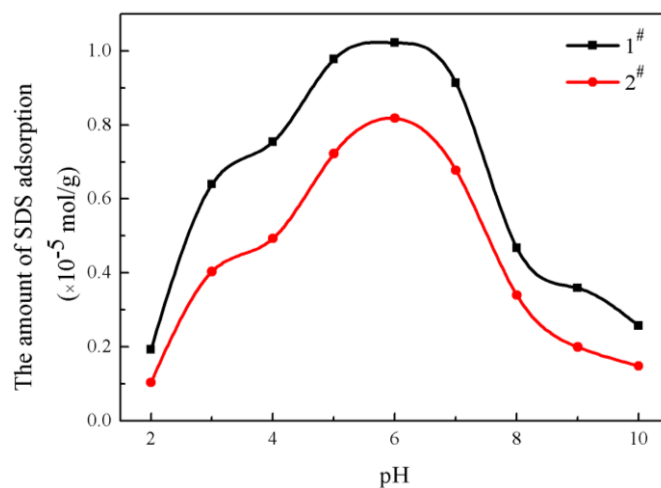


Fig. 9. Effect of pH on the amount of SDS adsorption

### 3.6 Capacity of collector adsorption

As can be seen from Fig. 9, the amount of SDS adsorbed on quartz first increased and then decreased with the increase of pH values. The amount reached the maximum at pH 6. In addition, the adsorption rate of SDS on 1# and 2# samples was similar. However, the amount of 1# adsorption was higher than

that of 2#. Iron ions hydrolyze in aqueous solutions and form various hydrolytic products. These products are adsorbed on the surface of quartz, affecting the electrical properties of quartz surface and the amount of adsorption of collectors on quartz surface. And quartz with poor floatability originally was activated by  $\text{Fe}^{3+}$  while SDS used as a collector. Due to the richer inclusions in sample 1#,  $\text{Fe}^{3+}$  presented a stronger activation than that of sample 2#. Thus, ascribed to the better adsorption ability of SDS on sample 1#, the greater flotation recovery was obtained than that of sample 2#.

### 3.7 Flotation performance

The effect of pulp pH on the recovery of the two samples was shown in Fig. 10. The recoveries of 1# and 2# increased with the increase of pH values from 2 to 6 while decreased with the increase of pH values from 6 to 10. Due to the similar mineral properties of 1# and 2#, it was also observed that the flotation recovery of two samples had a similar trend in the range of pH 2-10. However, the flotation performance of 1# was better compared to 2#, in good agreement with the capacity of collector adsorption. The results of flotation tests presented that SDS had excellent collecting capacity at pH 6, and the recoveries of 1# and 2# improved up to 96.59% and 83.39%, respectively. When pH values were 3, 7, and 8, the difference of flotation recovery between 1# and 2# was more than 30%. It can be seen from the flotation results that the content of fluid inclusions in quartz had an obvious effect on the flotation recovery.

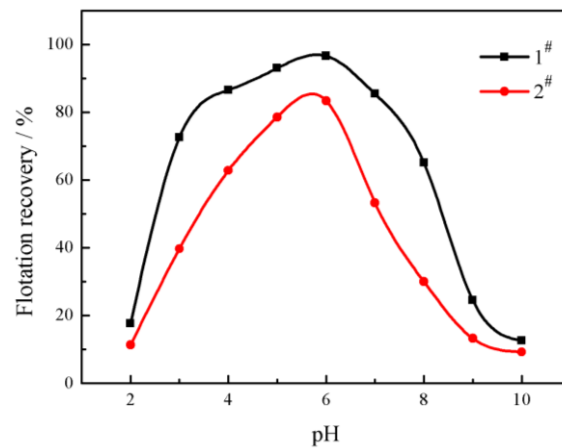


Fig. 10. Recoveries of 1# and 2# as a function of pH

### 3.8 Mechanism

It can be seen from Fig. 11 that metallic cations like  $\text{Fe}^{3+}$  can be adsorbed on the surface of quartz due to its negatively charged surface. Anionic collector SDS can be adsorbed on the quartz treated by  $\text{Fe}^{3+}$ . Based on the forgoing results, 1# has more abundant inclusions than 2#. The Zeta potential results showed that 1# had more negative potential, resulting in the stronger attraction to  $\text{Fe}^{3+}$ . The activation effect of Fe on 1# quartz was better, so more SDS was adsorbed on the surface of 1#. Furthermore, the froth layer of 1# was thicker and floated faster during the flotation process. The flotation results showed that when pH value was 6, the best pH value for flotation performance, the flotation recovery of 1# was 13.2% higher than that of 2#.

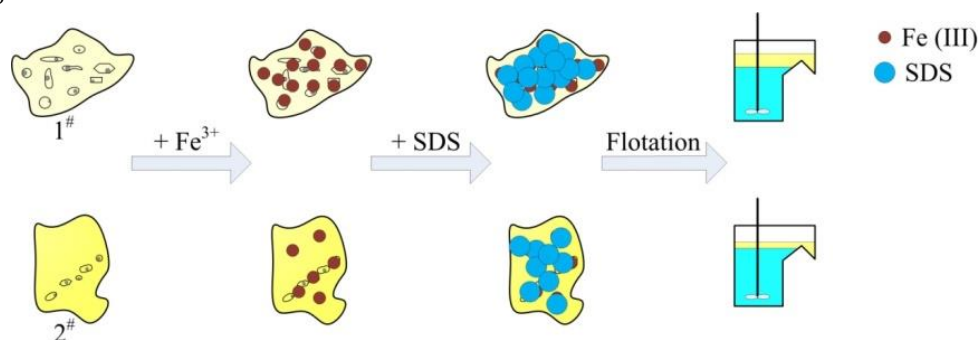


Fig. 11. Schematic diagram of quartz collected by SDS with activation of  $\text{Fe}^{3+}$

#### 4. Conclusions

It can be seen from the microscopic observation, large numbers of fluid inclusions with various sizes in 1#, while few fluid inclusions in 2#. Raman analyses indicated that both 1# and 2# were mainly as a gas-liquid phase. According to the sizes and numbers of fluid inclusions measured by the microscope, the fluid inclusion abundances for the two kinds of quartz were 0.42% for 1# and 0.11% for 2#.

The results presented in this work demonstrated that quartz with higher fluid inclusion abundance possessed more negative potential adsorbed more Fe<sup>3+</sup> and SDS on the surface compared to that with lower fluid inclusion abundance. Experimental results showed that recoveries of quartz were 96.59% for 1# and 83.39% for 2#, respectively, indicating that quartz with higher fluid inclusion abundance would be collected more effortless. All the findings illustrated that fluid inclusion in quartz is one of the factors affecting the surface characteristics and flotation behavior of quartz.

#### Acknowledgements

The authors would like to acknowledge the financial support from the funds for mega project of science research of Anhui Province (No. 15czz02044).

#### References

- ALLEN G. C., 2004. *X-ray photoelectron study of oxygen bonding in crystalline C-S-H phases*. Phys. Chem. Minerals, 31, 337-346.
- BODNAR R. J., 1993. *Revised equation and table for determining the freezing point depression of H<sub>2</sub>O-NaCl solutions*. Geochim. Cosmochim. Acta, 57, 683-684.
- BURKE E A. J., 2001. *Raman microspectrometry of fluid inclusions*. Lithos, 55, 139-158.
- CHANDRA A.P., GERSON A.R., 2009. *A review of the fundamental studies of the copper activation mechanisms for selective flotation of the sulfide minerals, sphalerite and pyrite*. Advanced Colloid Interface Science, 145, 97-110.
- DU F. H., LI J. S., LI X. X., ZHANG Z. Z., 2011. *Improvement of iron removal from silica sand using ultrasound-assisted oxalic acid*. Ultrason. Sonochem., 18, 389-393.
- DUBESSY J., BOIRON M., MOISSETTE A., MONNIN C., SRETENSKAYA N., 1992. *Determinations of water, hydrates and pH in fluid inclusions by micro-Raman spectrometry*. Eur. J. Mineral, 4, 885-894.
- FAN C. H., MA, H. R., HUA, L., WANG, J. H., WANG H. J., 2012. *FTIR and XPS Analysis of Characteristics of Synthesized Zeolite and Removal Mechanisms for Cr (III)*. Spectroscopy and Spectral Analysis, 32, 324-329. (in Chinese)
- GOLDSTEIN R. H., 2001. *Fluid inclusions in sedimentary and diagenetic systems*. Lithos, 55, 159-193.
- HOU Q., JING L., Yin R., CHEN L., LU L., JI F., 2012. *Study on Gas-Liquid Inclusions in Quartz Sand under Microwave Field*. Adv. Mater. Res, 689-693.
- HUANG P., FUERSTENAU D. W., 2001. *The effect of the adsorption of lead and cadmium ions on the interfacial behavior of quartz and talc*. Colloids Surfaces A Physicochem. Eng. Asp, 177, 147-156.
- KOH P. T. L., HAO F. P., SMITH L. K., CHAU T. T., BRUCKARD W. J., 2009. *The effect of particle shape and hydrophobicity in flotation*. Int. J. Miner. Proc., 93, 128-134.
- KRASOWSKA M., MALYSA K., 2007. *Kinetics of bubble collision and attachment to hydrophobic solids: effect of surface roughness*. Int. J. Miner. Proc., 81, 205-216.
- LARSEN E., KLEIV R. A., 2015. *Towards a new process for the flotation of quartz*. Miner. Eng., 83, 13-18.
- LI J., LI X., DU F., 2010. *Further Purification of Industrial Quartz by Much Milder Conditions and a Harmless Method*. Environ. Sci. Technol., 44, 7673-7677.
- LIU J., WEN, S., DENG J., CAO, Q., MILLER J. D., WANG X., 2013. *Contribution of fluid inclusions to variations in solution composition for sphalerite/quartz samples from the Yunnan Province, PRC*. Colloids Surfaces A Physicochem. Eng. Asp., 436, 287-293.
- LU H. Z. et al., 2004. *Fluid inclusions*. Beijing, China :Science Press.
- LUCE M., TECCE F., CASAGLI A., 2012. *Raman spectroscopy for fluid inclusion analysis*. J. Geochemical Explor., 112, 1-20.
- LUO B., ZHU Y., SUN C., LI Y., HAN Y., 2015. *Flotation and adsorption of a new collector  $\alpha$ -Bromodecanoic acid on quartz surface*. Miner. Eng, 77, 86-92.

- MOWLA D., KARIMI G., OSTADNEZHAD K., 2008. *Removal of hematite from silica sand ore by reverse flotation technique*. Sep. Purif. Technol., 58,419-423.
- NIE Y. M., LU X. L., NIU F. S., 2013. *Purification Experiment Research of Quartz Sand*. Appl. Mech. Mater., 389, 346-348.
- PARIS-NORD U., MOLTKULAIRE P., PARWSUD U., MOIPCULAIRE L. D. S.,1989. *Density effect on the Raman fermi resonance in the fluid phases of CO<sub>2</sub>*. Chem. Phys. Lett., 160, 250-256.
- PLATIAS S., VATALIS K. I., CHARALABIDIS G., 2013. *Innovative processing techniques for the production of a critical raw material the high purity quartz*. Procedia Econ. Financ, 5, 597-604.
- SAHOO H., RATHS. S., DAS B., 2014. *Use of the ionic liquid-tricaprylmethyl ammonium salicylate (TOMAS) as a flotation collector of quartz*. Sep. Purif. Technol., 136, 66-73.
- SANTOS M. F. M., FUJIWARA E., SCHENKEL E. A., ENZWEILER J., SUZUKI C. K., 2015. *Processing of quartz lumps rejected by silicon industry to obtain a raw material for silica glass*. Int. J. Miner. Process, 135, 65-70.
- TUNCUK A., AKCIL A., 2016. *Iron removal in production of purified quartz by hydrometallurgical process*. Int. J. Miner. Process, 153, 44-50.
- VAN DEN KERKHOF A. M., HEIN U.F., 2001. *Fluid inclusion petrography*. Lithos, 55, 27-47.
- VATALIS K. I., CHARALAMBIDES G., BENETIS N. P., 2015. *Market of high purity quartz innovative applications*. Procedia Econ. Financ, 24, 734-742.
- VAZIRI HASSAS B., CALISKAN H., GUVEN O., KARAKAS F., CINAR M., CELIK M. S., 2016. *Effect of roughness and shape factor on flotation characteristics of glass beads*. Colloids Surfaces A Physicochem. Eng. Asp., 492, 88-99.
- VEGLIO F., PASSARIELLO B., ABBRUZZESE C., 1999. *Iron Removal Process for High-Purity Silica Sands Production by Oxalic Acid Leaching*. Ind. Eng. Chem. Res., 38, 4443-4448.
- WANG Y. H., REN J. W., 2005. *The flotation of quartz from iron minerals with a combined quaternary ammonium salt*. Int. J. Miner. Proc., 77, 116-122.
- XIA W., 2017. *Role of particle shape in the floatability of mineral particle: An overview of recent advances*. Powder Technol., 317, 104-116.
- XU J. G., 1991. *Theory and practice of fluid inclusion micro-thermometry with infrared microscope within opaque minerals*. Geol. Sci. Technol. Inf., 10, 91-95. (in Chinese)
- ZHAI Q., 2010. *Catalytic kinetic spectrophotometric determination of sodium dodecyl sulphonate*. Instrum. Sci. Technol., 38, 135-142.
- ZHANG Z. Z., LI J. S., LI X. X., HUANG H. Q., ZHOU L. F., XIONG T. T., 2012. *High efficiency iron removal from quartz sand using phosphoric acid*. Int. J. Miner. Proc., 114-117, 30-34